Shock Detachment Process in Hypervelocity Flow over a Cone

I.A. Leyva, H.G. Hornung

Graduate Aeronautical Laboratories, California Institute of Technology, Pasadena, CA 91125, USA

Abstract: A comprehensive experimental and computational study of the shock detachment process in hypervelocity flow over cones is presented. The experiments are carried out in the T5 hypervelocity shock tunnel. The computations are mostly done with a code for axisymmetric thermo–chemical nonequilibrium flow. The data obtained confirm a previous theoretical model that predicts lower growth rate of the detachment distance with increasing cone half–angle for nonequilibrium flows than for frozen and equilibrium flows. The lower growth rate is related to the behavior of the sonic line in relaxing flows. The growth of the subsonic region is studied in detail from attached to detached conditions. A comparison between measured and computed interferograms is also made. Measured and computed heat flux distributions are compared, and differences between flows with attached and detached shocks are discussed.

Key words: Shock detachment, Hypervelocity flow, High enthalpy, Nonequilibrium cone flows

1. Introduction

The flow over cones at hypervelocity conditions is one of the most sensitive flows to thermo–chemical nonequilibrium. For certain combinations of free–stream conditions and cone half–angles, the shock can be detached if the flow is frozen but attached if the flow is in equilibrium. The rate of increase of the detachment distance with cone half–angle is strongly affected by the relaxation rate. Features of special interest are the conditions for incipient shock detachment, the important parameters of the body geometry and free–stream conditions that determine the detachment process, and the effect of shock detachment on heat loads and surface pressure. This knowledge can be applied to the design of inlets or any other sharp large–half–angle conical structure in a hypersonic vehicle.

The objective of the present study is to explain the effects of nonequilibrium on the shock detachment distance and its growth rate with increasing cone half–angle in hypervelocity flows. This work extends the study by Hornung and Houwing (1980) which showed that the growth rate of the detachment distance with increasing cone half angle is smaller for nonequilibruim than for frozen or equilibrium flows, and related this effect to the behavior of the sonic surface. The results were, however, only marginally conclusive because of the relatively large measurement uncertainties. With a greater range of free–stream conditions, coupled numerical investigation, higher resolution interferograms, and heat flux and surface pressure measurements, the present study has been able to yield conclusive results.

2. Experiments

About 170 shots have been performed in the T5 hypervelocity shock tunnel at Caltech, which is described in Hornung (1992). A total of 24 stainless steel cones have been tested, ranging in base diameter d from 2 cm to 16 cm and cone half–angles from 55° to 75°. Figure 1 shows a schematic diagram of a model in the test section of T5. The variable d_{ep} is the distance from the tip of the cone to the nozzle exit plane during the test time.

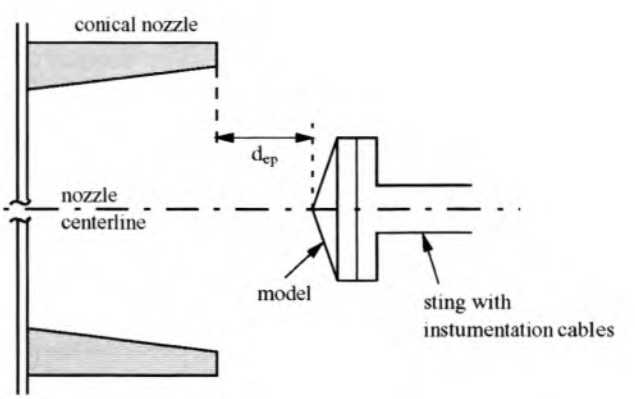

Figure 1. Schematic diagram of model in test section of T5.

The cones with $d = 8$ cm and $d = 16$ cm are instrumented with coaxial thermocouples and the largest cones also have recessed pressure transducers. Flow visualization by holographic interferometry gives quantitative field information and, in particular, the detach-

ment distance. Each cone is tested in six free–stream conditions (see tables 1 and 2) which span the available ranges of stagnation pressure and enthalpy of T5. The values of h_o and P_o represent the mean and standard deviation calculated from all the shots obtained for a given free–stream condition. All the shots are performed using a 7° half–angle conical nozzle.

Table 1. Free–stream conditions used.

Condition	N_2 1	N_2 2	N_2 3
h_o (MJ/kg)	18.2 ± 0.7	10.3 ± 0.9	16.3 ± 1.1
P_o (MPa)	53.6 ± 1.5	53.9 ± 2.8	20.3 ± 1.3

Table 2. Free–stream conditions used. (Cont'd.)

Condition	N_2 4	CO_2 2	CO_2 3
h_o (MJ/kg)	9.20 ± .38	6.62 ± 0.39	9.13 ± .46
P_o (MPa)	28.2 ± 1.5	24.5 ± 1.2	64.7 ± 1.8

3. Computations

The reservoir conditions in T5 are calculated using the computational tool STANJAN, see Reynolds (1986). For N_2 flows, the conical conditions at the nozzle exit are computed using the code SURF, see Rein (1989), for the conditions just downstream of the throat, and a modified version of the code by Olejniczak (1997) for the nozzle exit results. For CO_2 flows, the quasi–one–dimensional code NENZF, see Lordi et al. (1966), is used to calculate the nozzle exit conditions.

The main numerical code used to simulate cone flows was originally written by Candler (1988) and improved by Olejniczak (1997). It uses a finite–volume approximation to solve either the Navier–Stokes equations or the Euler equations for 2-D or axisymmetric flows with thermo–chemical nonequilibrium. The code can also be used for frozen flows. For the spatial differencing it uses a flux-splitting method, see Candler and MacCormack (1991), based on the Steger and Warming approach. The code marches in time using the implicit and iterative Gauss–Seidel line relaxation method. For this study, the vibrational modes are modeled as harmonic oscillators and the Park model is used for the vibration–dissociation coupling. The dissociation rates for N_2 are taken from Park (1985) and those for CO_2 flows are taken from Park et al. (1994). Almost all the grids for cones with d=8 cm or smaller have 100×200 cell points. The grids for the biggest cones have 200 × 200 points.

In a few cases, the computational system Amrita, see Quirk (1998), is also used to compute inviscid, frozen flows. This system provides the advantage of adaptive mesh refinement. For the cases run here, a flux–limited, operator split, Roe solver is used. The grids used have 120 × 200 cells, and two tiers of refinement by a factor of 3 are applied, giving an effective grid resolution of 1080×1800.

4. Theoretical considerations

On the basis of a simple scaling argument, Hornung and Houwing (1980) are able to deduce that the detachment distance Δ is scaled by the cone diameter (for a given free–stream condition and cone half–angle) for frozen and equilibrium flows. Nonequilibrium flows introduce a new length scale, the relaxation length l, which in this case is taken as an overall characteristic length for the vibrational and chemical relaxation processes. In the range of cone angles between the frozen and the equilibrium detachment angle, the detachment distance Δ is scaled by the relaxation length l. The ratio l/d is zero for equilibrium flows and infinite for frozen flows. The growth rate is expected to be smaller when the detachment distance is controlled by l than when it is controlled by d. This is related to the difference in the growth rate of the subsonic region inside and outside the relaxation zone. Hornung and Smith (1979) show that, within the relaxation zone, the frozen speed of sound decreases more rapidly than the flow speed with distance along a streamline. This means that, in this range of angles, a subsonic region is embedded in the relaxation zone, and the extent of this subsonic zone scales the detachment distance. The rate at which the detachment distance grows with angle in this range is therefore determined by the relaxation process.

5. Results and discussion

5.1. Sonic line from attached to detached conditions in frozen flows

If we start with a given free–stream condition and cone diameter, as we increase the cone half–angle, the flow will be supersonic throughout the shock layer up to a certain critical angle. A subsonic region then starts to grow from the cone surface and from near the cone tip. With further angle increase, the subsonic region grows toward the cone corner and toward the shock. Figure 2 left shows a numerical simulation of frozen flow with an attached shock and mixed supersonic–subsonic conditions. This simulation was performed with Amrita. The white line represents the sonic line. In order for the shock to detach, the sonic line has to reach the corner of the cone at its downstream end and the shock along its upstream face like in figure 2 right. It is then that the size of the cone can be communicated back to the tip of the cone and the detachment distance is scaled by d, as argued by Hornung and Houwing (1980). In these computa-

tions, it was found that the transition from attached to detached conditions is not abrupt. For the case studied here it took about 2.5° for the shock to detach after the sonic line had met the two conditions mentioned above.

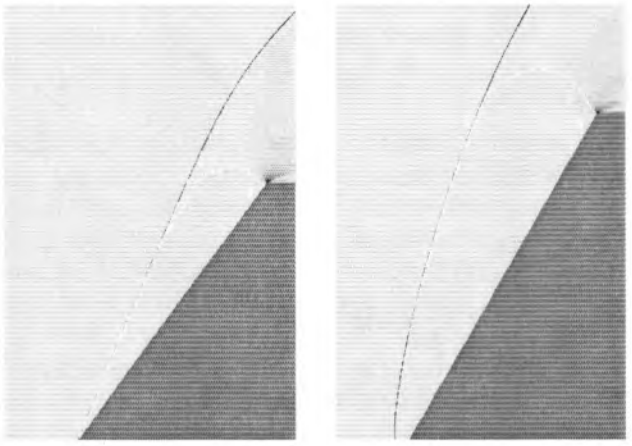

Figure 2. Left: Frozen flow with attached shock and mixed supersonic–subsonic conditions: $\theta = 53.8^\circ$ $M = 5.89$ $\gamma = 1.4$. Right: Frozen flow with detached shock. The sonic line has reached the corner of the cone on the downstream end and the shock in the upstream face: $\theta = 60.0^\circ$ $M = 5.89$ $\gamma = 1.4$

5.2. Experimental and computed interferograms

Figures 3 and 4 present a comparison between an experimental and a computed interferogram. Notice that the fringe distributuion in the experimental interferogram is asymmetric, with more dark fringes on the upper side. This asymmetry was a recurrent feature in those experimental interferograms for which the infinite–fringe condition was not achieved, so that fringes were evident in the free stream. Without taking into account the free–stream fringes, the computed interferograms show symmetric flow fields, as one would expect, since both the free stream and the cone flow are symmetric about the same axis. When the free–stream fringe distribution is taken into account in the computed interferogram, see figure 4, the flow field becomes asymmetric and the agreement in the number of fringes is also improved.

5.3. Dependence of detachment distance on relaxation rate

For given free–stream conditions, the relaxation length is approximately constant for the range of angles considered here. Thus, one way to vary the ratio l/d is by varying the diameter of the cone. Changing the cone diameter can make the flow go from near the frozen limit to near the equilibrium limit. Figure 5 shows a compilation of the normalized detachment distance for the free–stream condition N_2 4 and four cone

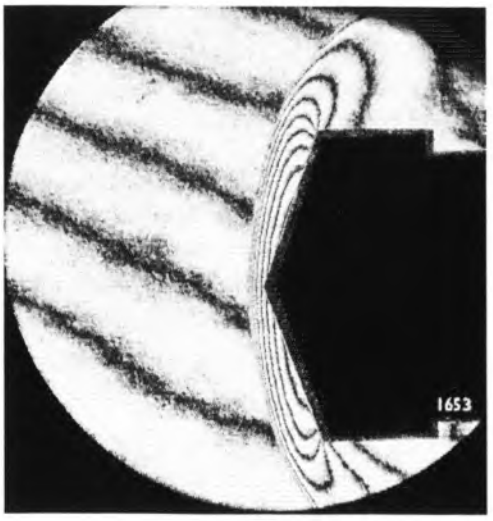

Figure 3. Experimental interferogram for condition N_2 2: $\theta = 70^\circ$ $d = 4$ cm.

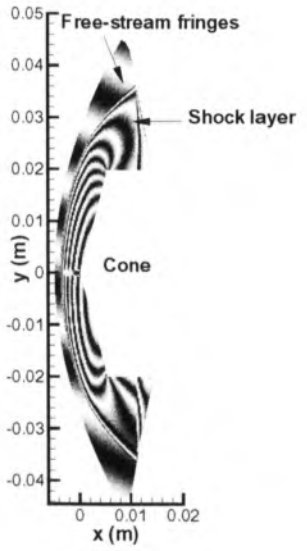

Figure 4. Computational interferogram for condition N_2 2: $\theta = 70^\circ$ $d = 4$ cm.

diameters. The results are plotted against the cone half–angle θ. The only data available for the frozen and equilibrium limits come from numerical simulations. The data labeled "f" are obtained from the code by Olejniczak (1997) run in its frozen inviscid mode. The data "f a" are also for the frozen limit but obtained with the Roe code under Amrita. The discrepancy between the two data sets is attributed to the uncertainty in the value of the effective γ for the free–stream condition. Both data sets are well fitted by straight lines confirming the experimental data of Ward and Pugh (1968). The data set "e" is obtained from numerical calculations for the equilibrium limit obtained with the code by Olejniczak (1997) by adjusting the reaction and relaxation rates appropri-

ately. The good linear fit to the frozen and equilibrium results confirm the features expected from the theory of Hornung and Houwing (1980). The points θ_f and θ_e are the critical detachment angles for frozen and equilibrium flow, respectively. The difference between these values increases with the fraction of the total energy of the flow that is absorbed by the relaxation, and therefore also increases with reservoir enthalpy. The curve "2cm" shows the experimental data obtained for the smallest diameter cones. As expected, this data set is closest to the frozen limit. In fact, this flow is almost frozen as revealed by the linear behavior of the curve and by the fact that the linear fit is good nearly all the way to incipient detachment. As the cone diameter increases, the curves shift toward the equilibrium limit. Notice that the dimensionless detachment distance grows more slowly for the relaxing flows than for the frozen and equilibrium flows as expected. Also note that all the curves start to detach from the same point (θ_f) as predicted by Hornung and Houwing (1980). The error bars represent the uncertainty in reading the detachment distance off the interferograms and the effect of the uncertainties in the free–stream on the detachment distance. For most of the N_2 conditions studied here, the discrepancy in Δ/d between experimental and numerical data is between 6 and 10%, with the computational data falling fairly consistently below the experimental values, however, the difference is too small to attach significance to it. Figure 6 is an example of the results obtained for CO_2 flows. The frozen data are again well fitted by a straight line as expected since the linear behavior is independent of the gas used. Notice how all the curves are closer to the equilibrium limit than for the N_2 example. Also note the larger separation between θ_f and θ_e. This is to be expected since the separation depends on the amount of energy absorbed by relaxation, which is greater for the CO_2 flows treated here than for the N_2 flows. The numerical simulations for CO_2 were not as successful as those for N_2. A more detailed model for the different vibrational modes in CO_2 is needed along with more accurate reaction rates and a nozzle code to take into account the conical nature of the free–stream flow.

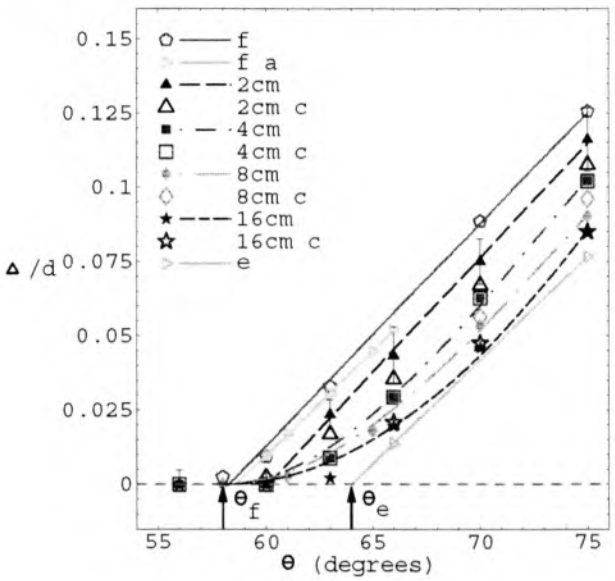

Figure 5. Non–dimensional detachment distance for condition N_2 4. The filled symbols indicate experimental results. The straight lines are linear fits to the numerical data "f", "f a", and "e", and to the experimental data set "2cm" . The rest of the curves are cubic fits to the experimental data presented to aid the eye. The letter "c" at the end stands for computations.

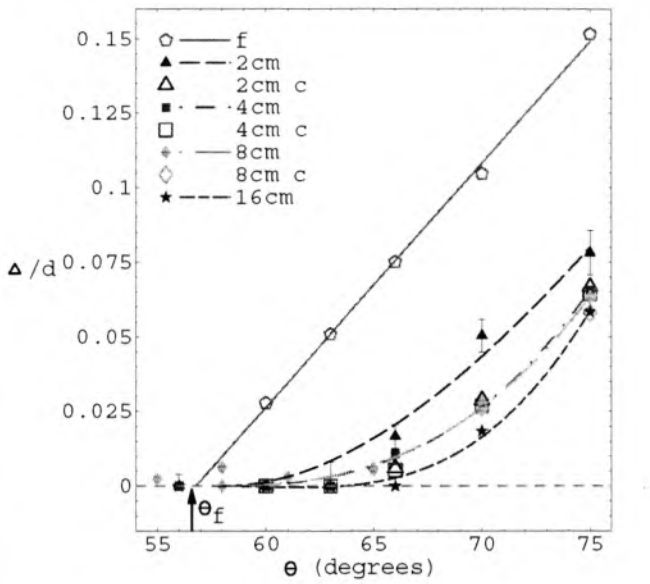

Figure 6. Non–dimensional detachment distance for condition CO_2 2. The filled symbols indicate experimental results. The straight line is a linear fit to the numerical data "f" while the rest of the curves are cubic fits to the experimental data presented to aid the eye. The letter "c" at the end stands for computations.

5.4. Normalized detachment distance from the frozen to equilibrium limits

In this section, we try to collapse the normalized detachment distance obtained for different N_2 conditions, from the frozen to the equilibrium limits, for a given cone half–angle. Using the ideas of Wen and Hornung (1995), who studied nonequilibrium flow over spheres, we now scale the dimensionless detachment distance by the density ratio across the frozen normal shock:

$$\Delta_m \equiv \frac{\Delta}{d}\frac{\rho_s}{\rho_\infty}, \qquad (1)$$

where the subscript s denotes conditions immediately after the shock and ρ_∞ is the free–stream density. We plot this variable against the reaction rate parameter Ω which quantifies the rate of energy absorption by relaxation. In this sense it is similar to the ratio l/d used previously. For N_2 flows Ω reduces to

$$\Omega \sim \frac{\rho_s d \left(\frac{\partial h}{\partial \alpha}\frac{d\alpha}{dt}\right)_s}{\rho_\infty u_\infty^3}, \qquad (2)$$

where α is the mass fraction of atomic nitrogen (N), h is the specific enthalpy, and u_∞ is the free–stream speed. This expression is evaluated assuming nitrogen to be well approximated by the ideal dissociating gas model. The results are presented in figure 7. In this case, $\Omega = 0$ represents the frozen limit and $\Omega = \infty$ represents the equilibrium limit. The different curves obtained for the same condition are the results of using different baseline diameters to numerically reach the frozen and the equilibrium limits as explained in Leyva (1999). If this flow followed binary scaling, as expected since the ratio of the dissociation to the recombination reaction rates varies from 500-5000 for the cases studied here, all the curves for a given condition would collapse into a single curve. We would have three curves instead of four. The differences between

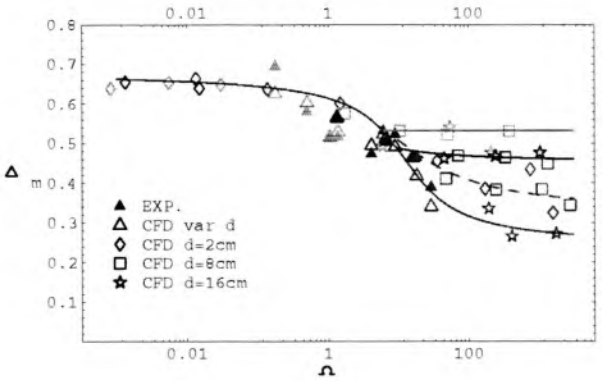

Figure 7. Modified non–dimensional detachment distance from frozen to equilibrium limits. The red color corresponds to condition N_2 3, green to condition N_2 4, and blue to condition N_2 2. The curves shown are fits of the form $y = A + B\arctan(cx + d)$ for the numerical data. For all of these cases the cone half–angle is 75°

the data sets for different diameters for a particular condition, as the equilibrium limit is approached, can be explained in terms of the experimental error, except for the difference between the curve "CFD d=16cm" and the curve for "CFD d=8cm" and "CFD d=2cm" for condition N_2 3. This difference is most probably due to vibrational non–equilibrium which is ignored while deriving the significant scaling parameters for binary scaling. We do observe, however, a collapse of the curves for different conditions in the frozen limit. Also observe that the detachment distance changes most rapidly for the range of cone diameters used in this study. This dramatic change means that we have captured the most sensitive regime for the effects of nonequilibrium on the detachment distance. The offset along the Ω–axis, in the fast–changing region, from one condition to another can be accounted for in terms of the error in Ω which is about 80%. Finally, the difference between the frozen and the equilibrium plateaus for each condition is proportional to the stagnation enthalpy of the condition as mentioned before.

5.5. Dimensionless heat flux and pressure distributions

Heat flux measurement are made to determine whether the heat flux is a sensitive indicator of shock detachment. The results are also compared with results from computations using the code by Olejniczak (1997) in its viscous mode. To non–dimensionalize the results, we form the Stanton number St, and the Reynolds number Re_x,

$$St = \frac{\dot{q}}{\rho_\infty u_\infty h_o}, \qquad (3)$$

$$Re_x = \frac{\rho_{eq} u_{eq} x}{\mu_{eq}}, \qquad (4)$$

where $\dot{q}$ is the dimensional heat flux, μ is the viscosity of the flow, and the subscript "eq" denotes properties evaluated in the stagnation streamline after the shock when the vibrational and translational temperature are in equilibrium. Figure 8 is a logarithmic plot of typical results obtained for a given N_2 condition for different cone diameters. The CFD data are fitted to straight lines in their linear part in the low Re limit. For attached shocks the slope of this line should be -1/2 , following the formula,

$$St = \frac{A}{\sqrt{Re}}, \qquad (5)$$

which applies for attached shocks, see Leyva (1999). In this case the slopes are 0.48 and 0.47 for the CFD data, even though equation 5 does not strictly apply anymore. If the heat flux were sensitive to the chemistry, we would see the effects in this graph, where the cone diameter changes by a factor of four. What we have instead are very similar curves in terms of the slope in the low Re limit and their general shape. The corner of the cone manifests itself in two ways, the most evident one is the heat flux peak near the corner. This peak is due to the thinning of the boundary layer as it approaches the expansion around the corner. The more subtle one is the "peel-off" of each curve from the linear behavior. As the size of the cone increases, the range of Re covered by the cone is larger and the heat flux follows the linear part of the curve longer before "feeling" the effects of the corner. Therefore,

the heat flux measured close to the end of the cone (before the corner peak) gets lower and lower as the cone diameter increases.

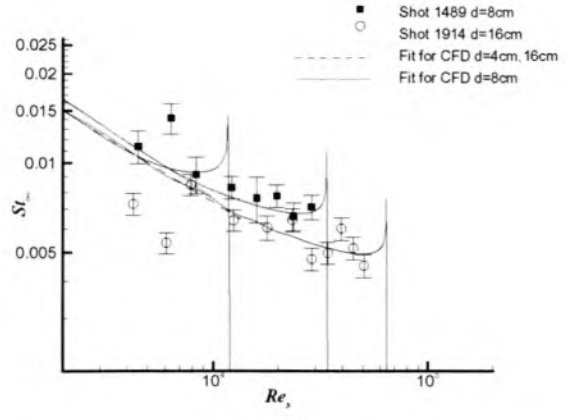

Figure 8. Comparison of non-dimensional heat flux for condition N_2 4.

The results obtained from the surface pressure measurements confirm the theoretical predictions that surface pressure is not sensitive to nonequilibrium effects. It was found that the numerical results slightly underpredict (less than 10%) the surface pressure measurements.

6. Conclusions

The shock detachment process on cones in hypervelocity flows has been studied experimentally and computationally. It has been confirmed that the detachment distance grows more slowly for relaxing flows than for frozen and equilibrium flows. The difference is due to the behavior of the sonic line inside and outside the relaxation zone behind the shock wave. The growth of the sonic line has been characterized from attached to detached conditions in the frozen case. It has been found that the transition from incipient to full detachment is not abrupt but takes a few degrees to be completed. The behavior of the detachment distance has also been characterized from the frozen to the equilibrium limits. A new modified detachment distance is correlated to the reaction rate parameter. The correlation is not perfect because of the effects of vibrational nonequilibrium. Measured and computed interferograms have also been compared. The heat flux distribution is found to be insensitive to shock detachment. The changes seen in the heat flux as the shock detaches can be attributed to the conditions at the edge of the boundary layer, the pressure field outside the boundary layer, and to the Reynolds number, rather than to nonequilibrium effects.

Acknowledgement. The authors would like to thank T5 members for helping to set up and run the experiments and Joe Olejniczak for providing the nonequilibrium code and endless help on its use.

References

Candler G (1988) The computation of weakly ionized hypersonic flows in thermo–chemical nonequilibrium. Ph. D. thesis, Stanford Univ

Candler GV, MacCormack (1991) Computation of weakly ionized hypersonic flows in thermo–chemical nonequilibrium. Journal of Thermophysics and Heat Transfer 5(3):266–273

Hornung, HG (1992) Performance data of the new free-piston shock tunnel at GALCIT. AIAA Paper 92-3943

Hornung HG, Houwing AFP (1996) Shock detachment from cones in a relaxing gas. Journal of Fluid Mechanics, 101:307–319

Hornung HG, Smith GH (1979) The influence of relaxation on shock detachment. Journal of Fluid Mechanics 93: 225–239

Leyva IA (1999) Shock detachment process on cones in hypervelocity flows. Ph. D. thesis, California Institute of Technology

Lordi JA, Mates RE, Moselle JR (1966) Computer program for solution of nonequilibrium expansions for reacting gas mixtures. NASA CR 472

Olejniczak J (1997) Computational and experimental study of nonequilibrium chemistry in hypersonic flows. Ph. D. thesis, University of Minnesota

Park C (1985) On convergence of computations of chemically reacting flows. AIAA paper 85-0247.

Park C, Howe JT, Jaffe RL, Candler GV (1994) Review of chemical-kinetic problems for future NASA missions, ii: Mars entries. AIAA Journal of Thermophysics and Heat Transfer, 8(1)

Quirk J (1998) Amrita— a computational facility (for CFD modelling). vonKarman Institute 29th CFD Lecture Series, ISSN 0377-8312

Rein M (1989) Surf: a program for calculating inviscid supersonic reacting flows in nozzles. California Institute of Technology, GALCIT FM 89-1

Reynolds WC (1986) The element potential method for chemical equilibrium analysis: implementation in the interactive program STANJAN. Stanford Univ Dept. of Mechanical Engineering Report

Ward C, Pugh PG (1968) Shock standoff distance of blunt and sharp cones. AIAA Journal, 6(10):2018–2019

Wen C-Y, Hornung HG (1995) Non-equilibrium dissociating flow over spheres. Journal of Fluid Mechanics 299:389–405